# THE NEW NIST LOW FROST-POINT HUMIDITY GENERATOR

Gregory E. Scace, Peter H. Huang, Joseph T. Hodges,
Douglas A. Olson and James R. Whetstone

Chemical Science and Technology Laboratory
National Institute of Standards and Technology
Gaithersburg, MD 20899

## ABSTRACT

We discuss the performance of a new high precision humidity generator designed to extend calibration capabilities at NIST from a lower concentration limit of 1.2·μmol/mol (−75 °C frost-point temperature) to 14 nmol/mol (−100 °C frost-point temperature) of water vapor. The system contains an ice-filled copper saturator residing within an evacuated enclosure. Without using liquid baths, the saturator temperature is actively regulated using thermoelectric devices and a mechanical refrigeration system for heat removal. Long-term stabilities on the order of 0.5 mK are demonstrated. Near-isothermal conditions within the saturator are achieved with high thermal conductivity materials, careful control of thermal boundary conditions and minimization of thermal loading from the laboratory environment. Maximum temperature differences in the saturator are less than 10 mK, and the uncertainty in temperature at the saturator outlet is estimated to be ~10 mK. We discuss some preliminary results of an intercomparison between the new generator and the NIST Mark−2 standard two-pressure generator. For the limited range of data studied, these agree to within the stated uncertainty of the two-pressure generator.

## INTRODUCTION

Over the last several decades, a number of moisture generators based on three different operating principles were developed at the National Bureau of Standards (NBS), now known as the National Institute of Standards and Technology (NIST). The three types, referred to as, two-flow, two-pressure and two-temperature generators were designed to be precision humidity generators suitable for use as national standards.[1]

Of the several moisture generators constructed at NBS, the current two-pressure apparatus known as the Mark−2 has been the most widely used system.[2] Designed and built in the early 1970's, it covers the range of frostpoint/dewpoint temperatures −75 °C to 40 °C. The Mark−2 has been used routinely for research purposes, and to calibrate hundreds of hygrometers used as transfer standards throughout the world. While its performance as precision generator is well-documented, it is bulky and expensive to operate. The most important limitation is its lowest achievable moisture concentration of about 1.2·μmol/mol, which is far greater than nmol-per-mol levels of moisture now of interest in many modern industries such as process gas and semiconductor manufacturing, meteorological and aerospace systems.

The demand for a standards-grade generator capable of reaching nmol-per-mol levels of humidity

*Presented at the 1997 NCSL Workshop and Symposium, Atlanta, GA, July 27-31, 1997*

motivated the present study. Here we present a novel two-temperature system, known as the Low Frost Point Generator (LFPG), designed to generate precise humidity levels in the frost-point temperature range −100 °C to −5 °C. Despite the significant overlap between the ranges of the LFPG and Mark−2, the former is not intended to replace the latter. Indeed, there are applications such as high flowrate calibrations or low-temperature relative humidity calibrations in which only the Mark−2 generator can be used. We note that a version of the LFPG, very different from that presented here, was built and tested at NBS over 25 years ago.[3] This system (now disassembled) was found to have an uncertainty in frost-point temperature near -50 °C of less than 200 mK based on intercomparison with the NBS Standard Gravimetric Hygrometer.[4]

Historically, the term two-temperature refers to generators in which air is saturated at one temperature, then raised to another known temperature to produce a mixture of fixed relative humidity. In our application, which is the generation of known concentrations of water vapor, the measurement of final temperature is unnecessary. The important distinction between two-pressure and two-temperature generators is that the latter saturates air at a known temperature and nominally ambient pressure, whereas the former saturates air at known temperature and at elevated pressure, expanding the air after saturation to produce the desired humidity level. While the LFPG normally operates as a two-temperature generator (in which the pressure drop between the saturator and hygrometer is negligible), it can also operate as a two-pressure generator if desired.

Initially, two generic types of humidity generators (flow-based and saturator-based systems) were considered. Flow-based generators depend on the mixing of wet and dry gas streams. Such systems, therefore require high accuracy in flow metering, whereas the output of a properly designed two-temperature system will, in principle, be independent of flowrate. This was considered to be a sufficiently compelling reason not to proceed with the development of a flow-based system. Of saturator-based generators, approaches based on two-pressure and two-temperature designs were compared. In two-pressure generators, moisture concentration can be changed quickly at fixed saturator temperature simply by varying the saturator pressure, whereas in two-temperature generators changes of setpoint can be slow since any change in the moisture concentration requires resetting to a new saturator temperature and waiting to reach thermal equilibrium. Also, frost-point temperatures well below the saturator temperature can be generated. Despite these advantages of two-pressure generators, we decided to build a two-temperature system for the following reasons. Two-temperature systems require no expansion valve to reduce the air pressure between saturator and hygrometer, and the downstream plumbing can be relatively short and simple. These simplifications eliminate potential uncontrollable water sources which can become problematic in the low concentration range. Also, unlike a two-pressure generator operated at high pressure, a two-temperature generator operated near atmospheric pressure does not suffer greatly from uncertainties in the enhancement factor (discussed below). For example, consider two generators, one a two-pressure system operated at $5 \cdot 10^5$ Pa and the other a two-temperature system producing air at the same frost-point temperature of −65 °C. Based on the analysis in Ref. 5, we estimate that the expanded uncertainties in generated water vapor concentration would be 1.7% and 0.9% for the respective generators.

The remainder of this paper is organized as follows. In the next section, we describe the physical basis of the humidity generation technique. Next, we continue with a detailed description of the apparatus, focusing on the critical aspects of the design. This is followed by a discussion of some measurements of parameters affecting the generator performance. Finally, we present some preliminary measurements in which we intercompare the LFPG with the Mark-2 two-pressure generator using a chilled mirror hygrometer, in the frost-point temperature range, -70 °C to -30 °C.

## PRINCIPLES OF OPERATION

The LFPG described here is designed to produce a gas stream of known water vapor content. In practice, a portion of this stream is monitored downstream of the generator by the hygrometer(s) under test. By ensuring that the inlet stream has reached thermodynamic equilibrium with the generator saturator, the water vapor concentration at the saturator outlet can be calculated from first principles. This requires knowledge of the relevant thermodynamic properties of water and carrier gas. With the additional assumption that there is no net change in water or carrier gas mass downstream of the saturator, the moisture content of the stream (expressed as a molar or mass fraction) at the test instrument is identical to that at the saturator outlet.

For the purpose of this discussion, we shall consider the generation of humidity in air streams. Assuming the air mixture to be invariant and inert, then one can treat the air-water system as a binary mixture. The thermodynamic state of such a binary homogeneous phase can be completely specified by means of its temperature, total pressure and the mole fraction of one component.[6] Within the saturator, the gas mixture is assumed to exist in thermodynamic equilibrium with the condensed phase, which for the LFPG, is essentially a single component system consisting of ordinary hexagonal ice. Equilibrium between the gaseous and condensed phases requires that the temperature and pressure of both phases be equal. Also, at equilibrium, any substance (such as water) passing freely between the two phases must have the same chemical potential within each phase.[7] Under these conditions, it can be shown that the mole fraction of water vapor in the gas phase, $x_w$, is proportional to the vapor pressure of the ice, $P_v(T)$, and the so-called enhancement factor $f(T,P)$.[8] At a total pressure, $P$, and system absolute temperature $T$, the mole fraction of water vapor is,

$$x_w = \frac{P_v(T)}{P} \cdot f(T,P) \quad , \tag{1}$$

where, $f(T,P)$, is a factor close to unity accounting for departures from ideal solution behavior as well as non-ideal gas effects. Hyland and Wexler give formulae for computing $f(T,P)$ in air-water systems.[9] The temperature dependence of the vapor pressure of ordinary hexagonal ice over the range (0 °C to -100 °C) was specified by Wexler.[10] This correlation, with the appropriate conversion from ITS-68 to ITS-90 [11] can be used to calculate $P_v(T)$. Combining the theoretical uncertainties reported by Wexler [10] and uncertainties based on measurements[12] of $P_v(T)$, we estimate the standard relative uncertainty in $P_v(T)$ to be 0.2 percent, 1 percent and 2 percent at 0 °C, -40 °C, and -70 °C, respectively. Equation (1) represents the central theoretical basis for the use of the low frost point generator as a moisture standard.

Measurements of the gas frost-point temperature made downstream of the saturator (as for example with a chilled mirror hygrometer) must be related to the saturator conditions. Assuming that the water vapor mole fraction is conserved, and assuming that the chilled mirror and sample stream are in local thermodynamic equilibrium, then,

$$x_w = \frac{P_v(T_s)}{P_s} \cdot f(T_s, P_s) = \frac{P_v(T_h)}{P_h} \cdot f(T_h, P_h) \quad , \tag{2}$$

in which the subscripts $s$, $h$ indicate conditions in the saturator and hygrometer respectively. Since $P_v(T)$ increases nonlinearly with $T$, this relation illustrates how isothermal expansion of the air leaving the saturator leads to a depression in the frost-point temperature.

## SYSTEM DESIGN, CONSTRUCTION AND OPERATION

A primary factor in the design of a two-temperature humidity generator is that temperature measurement and control dominates the overall system performance. In addition to describing the system, this section will address the level of temperature control achieved with the LFPG.

The LFPG as shown in Fig. 1 consists of a saturator residing within an evacuated enclosure, plumbing and flow control for the carrier gas, and associated temperature and pressure measuring instrumentation. A multi-mode closed-loop temperature control system maintains saturator temperature stability and eliminates the need for liquid temperature baths. Unlike liquid bath systems, this closed-loop temperature technique allows rapid adaptation to changes in heat loading. This temperature control system comprises thermoelectric devices (TEDs) which regulate the saturator temperature, and a mechanical refrigeration system which removes heat from the vacuum chamber.

Before entering the generator, carbon dioxide is removed from the test air which is then dried to a frost-point temperature near −73 °C. This humidity level is sufficiently dry to prevent ice from blocking the saturator passageways if the generator is operated for long periods at low temperatures. Downstream of the water-$CO_2$ removal system, the air enters a manifold where it may be diverted for flushing of the generator tubing or sent through the mass flow controller upstream of the saturator. This controller establishes the air flow rate (typically set to a nominal value of 2 ℓ/min) through the humidity generator. The metered air enters the saturator from top exiting the bottom on its way to the test instrument(s). After exiting the saturator, the test air passes through 1.5 m of electropolished tubing heated to 100 °C. This condition is established in anticipation of operation of the LFPG near its lower limit of −100 °C. The bulk of the test air bypasses the test instrument(s) through a back-pressure regulator which establishes the saturator air pressure. This air exhausts into the room environment. For two-temperature operation, the regulator is set to a pressure value satisfying the minimum pressure head required by the measuring instrument to meet its flow requirement for proper operation. In the case of most chilled-mirror hygrometers, the regulator is

atmospheric to 300 kPa absolute pressure. The remainder of the air flows to the test instrument(s).

Seven stacked, oxygen-free high-conductivity copper disks, each 195 mm in diameter and 18.5 mm thick, comprise the saturator. A diagram of the saturator with numbered disks is given in Fig. 2. Copper was chosen as the material for its high thermal conductivity and thermal diffusivity. Machined recesses in the outer faces of the top and bottom plates mate with two arrays (one on plate 1 and the other on plate 7) of four thermoelectric cooling devices per array. Plates 1 and 7 act as spacers between the TEDs and saturator passageway, and attenuate temperature gradients that might occur at the TED-saturator interface. Plates 2 through 5 contain the actual saturator. Spiral grooves, 9.5 mm wide by 9.5 mm deep, machined into the bottom faces of these plates form a passageway of square cross section, 4.88 m in length. Each spiral connects with adjacent spirals in the next plate of the saturator by vertical holes either at the center of the plate or at the outer end of the spiral. Air flows from the center of plate 2 to the outer end of the spiral, down into plate 3, to the center of plate 3, down to plate 4, to the outer end of the spiral, down to plate 5, to the center of plate 5, then down axially through plate 6 and out of the saturator. At each junction between saturator stages, a copper tube is pressed into a counterbore in the vertical hole, protruding 2.5 mm above the floor of the spiral passageway upstream of the hole. This tube forms a weir, damming liquid water during the saturator filling operation and evenly dispersing water throughout each stage of the saturator. In plate 6, a thermometer well, drilled radially with its centerline 7 mm below the bottom of plate 5 accommodates a 25 Ω encapsulated standards-grade platinum resistance thermometer (SPRT). A pressure tap runs radially to the center of plate 6. All seven plates were electroless nickel plated for corrosion resistance and vacuum furnace brazed using the nickel plating as the brazing filler material. This method of joining reduces the number of thermal contact resistances at each joined copper plate from four, as would be the case using conventional copper-silver brazing alloy, to two.

Axial conduction to and from the saturator is controlled by adding or removing heat via a multi-mode process. The two TED arrays, symmetrically located on plates 1 and 7 of the saturator, pump heat to or from the saturator as required to maintain a desired temperature. A digital multimeter in four-wire resistance mode measures the resistances of two 100 Ω SPRTs, embedded in the saturator near the top and bottom faces. These thermometers were calibrated by the NIST Thermometry Group and at that time had an expanded uncertainty below 1 mK (coverage factor of two). Using these temperature data as feedback in a servo-loop, two proportional-integral-derivative (PID) control algorithms are implemented via a computer interface to control the currents to the upper and lower TED arrays. The algorithms maintain temperature uniformity by minimizing the difference in temperature of the top and bottom saturator faces and by simultaneously minimizing the difference between the average of the top and bottom face temperatures and the setpoint temperature. Heat pumped from the saturator is removed from the vacuum environment via a mechanical refrigeration system. The refrigerant fluid, liquefied ethylene, is pumped to a pair of cylindrical refrigeration plates in contact with the TEDs. The liquid vaporizes in spiral passageways within the refrigeration plates and returns to a compressor and heat exchanger outside the vacuum chamber. An independent PID controller within the refrigeration system maintains the desired refrigeration plate temperature. When possible, the refrigeration plates are cooled to a temperature slightly below that of the saturator so that the TEDs pump heat to the saturator. Waste heat due to inefficiency of the TEDs is then used

to warm the saturator rather than burden the refrigeration system with its removal. At very low saturator temperatures, the TEDs are used as coolers, extending the temperature range of the saturator beyond the −97 °C temperature limit of the refrigeration system.

To minimize all other modes of heat transfer, the saturator resides in a vacuum chamber maintained at approximately $8 \cdot 10^{-4}$ Pa ($6 \cdot 10^{-6}$ torr) ; a pressure that is sufficiently low to effectively eliminate molecular heat conduction and gas phase heat convection within the vacuum chamber. Three radiation shields encircling the saturator (two of copper and one of aluminized polymeric film) minimize radiation heat transfer from the vacuum chamber walls to the saturator. An insulated box surrounds the evacuated enclosure to provide additional thermal resistance between the saturator and laboratory environment.

Unavoidable thermal conductive pathways are also minimized. The saturator itself rests on top of the lower refrigeration plate which is supported by three hollow legs threaded into an aluminum ring shrunk onto the refrigeration plate. Spherical ends of the legs fit into conical holes in the vacuum chamber walls, forming an annular contact ring of small surface area. Any heat that does travel up the legs is removed by the refrigerant within the refrigeration plate and does not reach the saturator. Heat conduction along the pressure sensing tube is minimized through the use of 3 mm o.d., 0.5 mm wall thickness tubing, and a long conduction path length (~3 m) within the evacuated enclosure. The inlet and outlet tubes constitute unavoidable heat leakage paths. While the conduction path length of the inlet tube can be quite long, the outlet tube must be as short as possible to minimize water adsorption and desorption effects downstream of the saturator. These tubes are located along the center axis of the saturator, so that their effect on the temperature distribution in the saturator is axi-symmetric. They are deliberately placed in close proximity to the TED arrays which remove the parasitic heat.

By monitoring the transient warmup of the saturator after turning off the temperature controlling systems, we demonstrated that the system has a high degree of thermal isolation from the surroundings. Near −100 °C, the rate of change of saturator temperature was measured to be ≈0.5 mK/s. This translates into a thermal loading on the order of 10 W.

As discussed earlier, frost-point temperature prediction requires knowledge of previously established values of temperature-dependent ice vapor pressure and temperature- and pressure-dependent enhancement factors. To calculate the frost-point temperature sensed by a chilled mirror hygrometer the pressure at the mirror must also be known. In practice the hygrometer pressure is closely approximated by the room pressure. Thus, using a chilled mirror hygrometer, accurate measurements of saturator temperature and pressure as well as barometric pressure are required. See Eq. 2. A quartz Bourdon tube pressure gage (range 0 - 300 kPa) measures the absolute gas pressure at the saturator outlet, and the ambient pressure is measured by a piezo-resistive gage. Both pressure gages are calibrated with a dead weight testing system having an expanded uncertainty of $40 \cdot 10^{-6}$ (coverage factor of two) and their analog outputs are read by a digital multimeter.

A 25 Ω SPRT, oriented radially in plate 6 and adjacent to the last stage of the saturator, is used to

define the saturator temperature. To minimize temperature gradients along the thermometer leads near the probe, the 25 Ω thermometer leads, as well as those of the control thermometers, are thermally anchored to the saturator by winding and cementing the leads to copper bobbins screwed to the saturator perimeter. The leads between the bobbins and thermometers are hidden behind the radiation shields to minimize radiation exchange between them and the vacuum chamber walls. The resistance of the 25 Ω thermometer is determined through comparison with a 100 Ω standard resistor, by multiplying the resistance of the latter by the ratio of measured voltage drops across the two resistances at a constant current of ~1 mA (which is the current at which the SPRT was calibrated). The standard resistor resides in a temperature controlled chamber at 36 °C ±0.1 °C. To eliminate thermal emf effects, the relevant voltages are measured in the forward and reverse current directions. An analysis of the sources of error using this technique shows that the uncertainty in the temperature measurement is driven by the stability of the current source. We measured its short-term stability and estimate a fractional uncertainty therein of $2.8 \cdot 10^{-6}$. The expanded uncertainty (coverage factor of two) of the temperature measurement using the 25 Ω SPRT is a function of temperature. The uncertainty arises from three sources; current instability, linearity of the multimeter and the expanded uncertainty of the thermometer calibration. For temperatures equal to −100 °C, −50 °C and 0 °C, the expanded uncertainties are, 1.7 mK, 2.3 mK and 2.8 mK, respectively. These uncertainties are in the temperature measurement procedure only, however. The overall saturator temperature uncertainty must also incorporate the implications of thermal gradients. This issue is discussed below.

## GENERATOR PERFORMANCE

Stability and Thermometry

The saturator temperature stability is limited by the speed, resolution and stability of the digital multimeter used to measure the control thermometer resistance, and by the ability of the TED control system to keep up with short-term changes in the heat load. Pulsing of refrigerant through the refrigeration plates, which is dictated by the refrigeration system's temperature controller, changes the temperature at the TED-refrigeration plate interface and the current required to maintain constant temperature at the TED-saturator interface. The controller updates the current supplied to each TED array every seven seconds, which is the time required to measure the resistance of the two control thermometers in both forward current and reverse current mode and to calculate the new current requirements. As shown below, this cycle time is sufficiently rapid to yield a temperature stability which is better than 2 mK about the setpoint.

A typical system temperature response at a setpoint temperature of −89.2 °C is shown in Figs. 3a-b, corresponding to the "average" and "difference" modes of control, respectively. In the average mode, the error signal is the difference between the average of the top and bottom saturator temperatures, as measured by the control thermometers and the setpoint temperature. Likewise, the error signal in the difference mode is equal to the upper minus the lower saturator temperatures as measured by the control thermometers. For these data, acquired over a four hour period, the maximum indicated error in the average mode was less than 2 mK. The distribution of error signals, see Figs. 3c-d, is very nearly Gaussian for both cases. In the average mode, the mean value is

-0.004 mK, with a standard deviation of 0.34 mK. The difference mode results, shown in Fig. 3d, have a mean value of 0.018 mK and a standard deviation of 0.81 mK. We note, however, that long term stability of the saturator temperature is primarily influenced by the stability of the multimeter used to measure the control thermometer resistances. Specifically, the manufacturer's stated 90 day stability of the multimeter in four-wire resistance mode is ±0.0064 Ω, corresponding to ±16 mK. Nevertheless, during four days of continuous operation near -99 °C, the saturator temperature as measured by the 25Ω SPRT remained constant to within 0.5 mK.

Temperature gradients within the saturator were measured by a pair of calibrated platinum resistance thermometers. The temperatures were measured throughout the operating range of the generator. First, to verify agreement between the thermometers, they were placed approximately 1 cm apart (center to center) in adjacent thermometer wells within the saturator. Next, one thermometer was moved to a well close to the saturator's pressure tap; the position deemed the most likely source of parasitic heat. In this configuration, the measured temperature difference between the two thermometers was less than 10 mK throughout the operating range of the generator. Since these measurements were taken, additional radiation shields have been installed around the saturator's perimeter. We have not yet repeated these measurements but expect the shields to reduce the saturator temperature gradients. Based on numerical simulations of heat transfer within the saturator, maximum temperature differences of about 3 mK at a setpoint temperature of -100 °C are expected. Until the temperature gradient measurements are revisited, we assign a value of 10 mK as a conservative estimate of the maximum temperature difference within the saturator.

Pressure Measurement

As previously mentioned, the quartz Bourdon tube pressure gage was calibrated using a piston gage calibrated by the NIST Pressure and Vacuum Group. The voltage output from the pressure gage was fit to the pressure produced by the piston gage. We estimate the fractional uncertainty due to the residuals of this fit to be $29 \cdot 10^{-6}$. At nominally atmospheric pressure, the manufacturer's stated one year accuracy for the voltmeter measuring output from the pressure gage is $34 \cdot 10^{-6}$. Identical pressure gages to ours with long term histories of calibration by the NIST Pressure and Vacuum Group typically exhibit 1 year drift of less than $100 \cdot 10^{-6}$. Lacking calibration history for our particular gage, we expect that it should perform on par with those of the Pressure and Vacuum Group and therefore assign $100 \cdot 10^{-6}$ as the uncertainty due to instrument drift. Our estimate of the expanded uncertainty (coverage factor of two) in the saturator pressure measurement is 12 Pa.

As discussed later in this paper, the pressure drop across the saturator will tend to slightly undersaturate the exiting air. This pressure drop is not considered in our uncertainty estimate since the relevant pressure is the pressure of the saturated gas stream at the location where ice coating terminates within the saturator passageway.

For calculation of frost-point temperature, the gas pressure at the hygrometer sensor must also be measured. Since the mirror of most chilled mirror hygrometers resides in a chamber which exhausts through a short length of tubing to the room, the ambient pressure is substituted for this pressure. An estimate of the pressure drop through a typical exhaust tube, 0.5 m long with an internal diameter

of 4.5 mm, at a flowrate of 0.67 ℓ/min, is 10 Pa. The piezo-resistive gage, which measures the barometric pressure, was calibrated at a pressure of 103 kPa using the dead weight tester described above. Uncertainties in ambient pressure were estimated in a similar manner to the analysis of the quartz Bourdon pressure gage described above and found to be 13 Pa.

Heat and Mass Transfer Effects

The air stream must spend sufficient time in contact with the ice and saturator walls for it to be at the saturator temperature and for it to be fully saturated with water vapor at the outlet. To assess whether the exiting air and saturator are in thermal equilibrium, we estimated the air and ice temperature as a function of distance along the saturator passageway using a one-dimensional steady state heat transfer model. Except at the highest saturator temperatures, energy fluxes associated with sublimation and condensation of water vapor are negligible when compared to the sensible heat exchange associated with cooling the carrier gas. The calculations based on the model suggest that the system behaves as a nearly perfectly efficient heat exchanger by virtue of its relatively low thermal resistance and the long residence time of the air. As the gas proceeds downstream, its mean temperature undergoes an exponential decrease, approaching the temperature of the saturator. For example, at a setpoint temperature of −100 °C and flowrate of 2 ℓ/min the characteristic decay length is about 19 cm. With a saturator length of 4.88 m, which corresponds to more than 25 decay lengths, temperature differences between the exiting air and saturator can be safely neglected. Also, to the extent that small temperature gradients exist in the flow direction, this relatively short decay length means that the temperature of the air exiting the saturator will be in local equilibrium with conditions near the saturator outlet. This supports the assumption that the 25 Ω SPRT (which resides in the last stage of the saturator) should be at a temperature close to that of the exiting air.

Johnson [13] analyzed mass transfer under laminar flow conditions in the saturator of the old NBS frost point generator and showed that once fully developed conditions are achieved, a radial distribution of water vapor concentration will develop within the saturator passageway as a consequence of fluid expansion in the flow direction. This effect leads to slight undersaturation of the stream exiting the saturator. Johnson showed that the degree of undersaturation is proportional to the pressure gradient in the flow direction.[13] In order to estimate the magnitude of this effect, we measured the pressure drop in the saturator at three saturator setpoint temperatures spanning the operational range of the generator. This was realized by connecting a capacitance diaphragm pressure gage, having an operating range of 0 to 133 Pa differential pressure, across the saturator's water inlet and the pressure tap at the saturator exit. The measurements at a flowrate of 2 ℓ/min and derived results based on Johnson's algorithm, are given in Table 1. At fixed mass flowrate, the pressure drop tends to grow with increasing saturator temperature due to increasing air viscosity. However, these results indicate that the expansion effect is likely to be very small. In the worst case, it causes approximately $184 \cdot 10^{-6}$ degree of unsaturation (defined below), or equivalently 2.2 mK of saturator frost point depression.

| *Saturator temperature* | *Pressure drop* | *Pressure gradient* | *Degree of unsaturation* | *Reduction in frost-point temperature* |
|---|---|---|---|---|
| (°C) | (Pa) | (Pa/m) | | (mK) |
| -10.0 | 40 | 8.05 | $184 \cdot 10^{-6}$ | 2.2 |
| -60.0 | 31 | 6.24 | $172 \cdot 10^{-6}$ | 1.3 |
| -98.5 | 24 | 4.83 | $139 \cdot 10^{-6}$ | 0.7 |

Table 1. *Measured mean pressure gradient in saturator at a flowrate of 2 ℓ/min of air. The degree of unsaturation, is defined as* $1 - \bar{C}/C_{sat}$ *where* $\bar{C}$ *is the mean water vapor concentration of the exiting stream and* $C_{sat}$ *is the saturated value. This was calculated using the algorithm given by Johnson.*[13]

Intercomparison with the NIST Two-Pressure Humidity Generator,Mark-2

As a preliminary assessment of the accuracy of the LFPG, we intercompared the LFPG with the NIST Two-Pressure Humidity Generator, (2-P) using a chilled mirror hygrometer as a transfer device. The 2-P generator is a well-characterized system whose output has been measured using the NBS Standard Gravimetric Hygrometer down to a frost-point temperature of -20 °C. [2] The maximum expanded uncertainties (coverage factor of two) of the 2-P generator are ±50 mK above -20°C frost-point temperature, ±70 mK between -20°C and -40°C, and ±140 mK for frost-point temperatures below -40°C. [5]

First, the hygrometer was calibrated several times over a three year period at irregular intervals against the 2-P generator. The mean resistance of the platinum resistance thermometer (PRT) adjacent to the hygrometer mirror was measured at 5 °C increments in the generated frost-point over the range -5 °C to -70 °C. These resistance data were fit by the method of least-squares to the generator frost-point temperature using the so-called Callender-Van Dusen (CVD) equation, a fourth-order polynomial given by,[14]

$$R_{CVD}(R_o, a, b, c; t) = R_0[1 + at + bt^2 + ct^3(t - 100^oC)] \qquad (3)$$

in which $(R_0, a, b, c)$ is a set of constants, and $t$ is the thermometer temperature. Note, in this analysis all temperatures are assumed to be in degrees Celsius. The CVD formula is a response function for industrial-grade PRTs which is specified by the standard ASTM-E 1137-95.[14] Along with the functional form of the PRT response function, this standard specifies a set of four generic values for the fit coefficients, $(R_0, a, b, c) = (R_{0,g}, a_g, b_g, c_g)$, and the associated temperature tolerances of the resulting fit.

We define the temperature residual, $\delta t_{i,2-P}(t_i, R_i)$, of the data pair, $(t_i, R_i)$, as the difference between the fitted temperature (obtained by inverting Eq. (3) to obtain a temperature at a measured value of

resistance) and the predicted frost-point temperature of the 2-P. The terms, $t_i$ and $R_i$, are the predicted frost-point temperature of the 2-P generator (at the hygrometer), and the measured resistance of the chilled mirror hygrometer, respectively. Thus,

$$\delta t_{i,2-P}(t_i, R_i) = t_{CVD}(R_0, a, b, c; R_i) - t_i \,, \tag{4}$$

where $t_{CVD}(R_0, a, b, c; R_i)$ is the inverse of the CVD function, and $(R_0, a, b, c)$ are the four CVD coefficients obtained by fitting the chilled mirror hygrometer vs. 2-P generator calibration data.

The temperature residuals $\delta t_{i,2-P}(t_i, R_i)$, (indicated by the symbols) for this calibration are shown in Fig. 4. The CVD fit of the chilled mirror vs. 2-P calibration data gave $(R_0, a, b, c)$=(100.06036Ω, $3.9056502 \cdot 10^{-3}$/°C, $-7.4661903 \cdot 10^{-7}$/°C$^2$, $1.9745613 \cdot 10^{-11}$/°C$^4$). Also shown in this figure, is a smooth line that corresponds to a third-order polynomial least-squares fit to the temperature residuals. This fit, which we designate by $\delta t_{2-P}(q_0, q_1, q_2, q_3; t)$, serves as an interpolating function that allows estimation of the temperature residuals at arbitrary frost-point temperatures over the range of the fit. The temperature residuals predicted by the CVD fit are well within the expanded uncertainties of the 2-P generator. Also, the CVD coefficients obtained here are very similar to the generic values specified by ASTM-E 1137-95.[14] The relatively small residuals of the CVD fit indicate that the response of the chilled mirror hygrometer is dominated by the thermometer behavior within the environment of the mirror.

The chilled mirror hygrometer was then connected to the output of the LFPG and its mean resistance, $R_j$, was measured at 10 °C intervals in frost-point temperature, $t_j$, from −30 °C to −70 °C. We define the measured frost-point temperature deviation at the LFPG to be,

$$\delta t_{j,LFPG}(t_j, R_j) = t_{CVD}(R_0, a, b, c; R_j) - t_j \,, \tag{5}$$

This temperature deviation was calculated at each LFPG test point $(t_j, R_j)$. Using the interpolating function, $\delta t_{2-P}(q_0, q_1, q_2, q_3; t)$, to estimate the temperature residuals of the 2-P generator at the observed LFPG frost-point temperatures, $t_j$, we define the difference between the 2-P temperature residuals and the measured frost-point temperature deviation at the LFPG to be,

$$\delta t_{(LFPG)-(2-P)}(t_j, R_j) = \delta t_{2-P}(q_0, q_1, q_2, q_3; t_j) - \delta t_{j,LFPG}(t_j, R_j) \,. \tag{6}$$

This quantity, shown in Fig. 5, is a measure of the agreement between the two generators. As defined, it is essentially independent of the functional form of the fitting equation used in the calibration of the transfer device since the fit-dependent terms in Eqs. (4) and (5) tend to cancel. For all frost-point temperatures considered, the agreement between the two generators falls within the expanded uncertainty of the 2-P generator.

At lower temperatures, the 2-P generator data exhibit more scatter, which may be attributed in part to the behavior of the hygrometer near its operational limit. Moreover, the limited number of samples obtained with the LFPG makes it difficult to assess the uncertainty in these data, especially

in the low temperature regime. Indeed, many more data points are required to complete this intercomparison between the LFPG and 2-P generators.

## CONCLUSION

The LFPG is a precision system capable of operating for long periods of time with minimal operator attention. During the course of the experiments described here, the generator operated reliably and without interruption for over two months. Thus, with a more extensive experimental characterization and uncertainty analysis, the LFPG will be a robust and precise humidity standard and research instrument. It extends NIST calibration capabilities to include precision nmol/mol-level hygrometers. Furthermore, its stability and inherent reliability will allow accurate gravimetric measurements requiring long (on the order of months) sampling times. Based on the collection over a two month period of 0.5 g of water at a flowrate of 2 ℓ/min, gravimetric measurements could conceivably be made down to frost-point temperatures as low as −65 °C (concentration of 5 μmol/mol). Such measurements should improve the accuracy of ice vapor pressure vs. temperature correlations currently in use. In addition, the LFPG will facilitate new humidity measurement techniques and low concentration humidity standards currently under development at NIST.[15,16]

## ACKNOWLEDGMENTS

We would like to thank R. Cutkosky for developing the PID-control algorithm used to drive the TED arrays. Also, we take this opportunity to thank R. Hyland, J.P. Looney, R.I. Scace and G. J. Rosasco for carefully reading the manuscript and offering many helpful suggestions.

## REFERENCES

1. S. Hasegawa, "National basis of accuracy in humidity measurements," ISA Trans., **25**, 15-24 (1986).

2. S. Hasegawa and J.W. Little, "The NBS two-pressure humidity generator, Mark-2," Jour. Res. NBS, **81A**, 81-88 (1977).

3. L. Greenspan, "Low frost-point humidity generator," Jour. Res. NBS, **77A**, 671-677 (1973).

4. A. Wexler and R.W. Hyland, "The NBS standard hygrometer," NBS Monograph 73, 1964.

5. P.H. Huang, "Determining uncertainties in standard dew/frost-point generators for humidity measurements," Proceedings of TEMPMEKO '96, Torino Italy, IMEKO TC12, (in press).

6. K. Denbigh, *The Principles of Chemical Equilibrium*, (Cambridge University Press, Cambridge England, Fourth ed., 1981), Chap. 7.

7. Ref. 6 Chap. 5.

8. R.W. Hyland and A. Wexler, "The enhancement of water vapor in carbon dioxide-free air at 30, 40, and 50 °C," Jour. Res. NBS, **77A**, 115-131 (1973).

9. R.W. Hyland and A. Wexler, "Formulations for the thermodynamic properties of dry air from 173.15 K to 473.15 K, and of saturated moist air from 173.15 K to 372.15 K, at pressures to 5 MPa,"ASHRAE Trans., **89**, 520-535 (1983).

10. A. Wexler, "Vapor pressure formulation for ice," Jour. Res. NBS, **81A**, 5-19 (1977).

11. H. Preston-Thomas and T.J. Quinn, *Techniques for Approximating the International Temperature Scale of 1990*, (Bureau International des Poids et Mésures, Pavillon de Breteuil, F-92310 Sèvres, First ed, 1990), Appendix A.

12. J. Marti and K. Mauersberger, "A survey and new measurements of ice vapor pressure at temperatures between 170 and 250 K," Geophys. Res. Lett., **20**, 363-366 (1993).

13. D.P. Johnson, "Note on diffusion of vapor into flowing gas," Jour. Res. NBS, **78A**, 49-51 (1974).

14. "Standard specification for industrial platinum resistance thermometers," ASTM std. designation E 1137-95, 1995.

15. J.T. Hodges, J.P. Looney and R.D. van Zee, "Laser bandwidth effects in quantitative cavity ring-down spectroscopy," Appl. Opt., **35**, 4112-4116 (1996)

16. J.T. Hodges, J.P. Looney and R.D. van Zee, "Response of a ring-down cavity to an arbitrary excitation," J. Chem. Phys., **105**, 10278-10288 (1996).

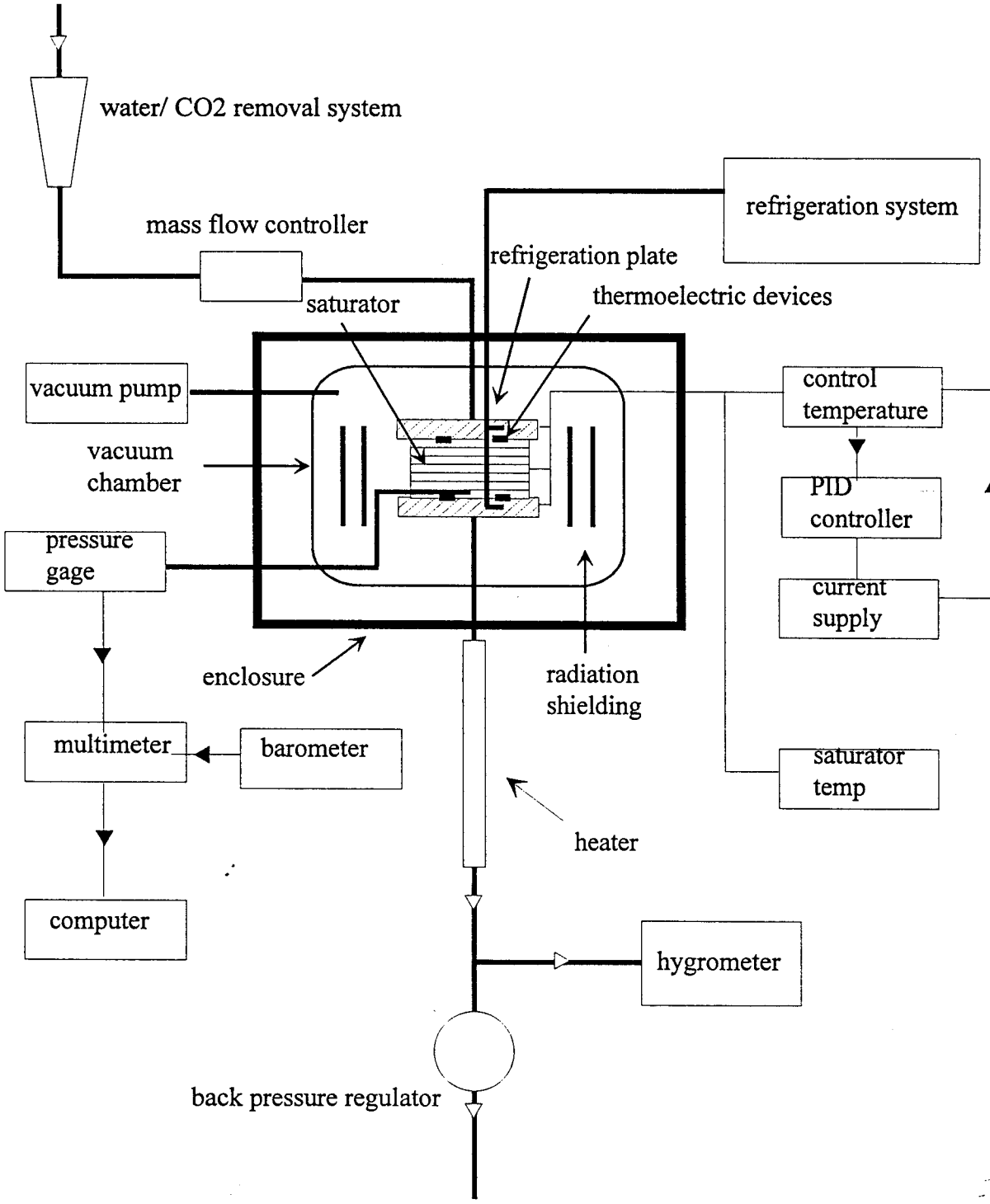


Fig. 1 Schematic of the Low Frost Point Generator system.

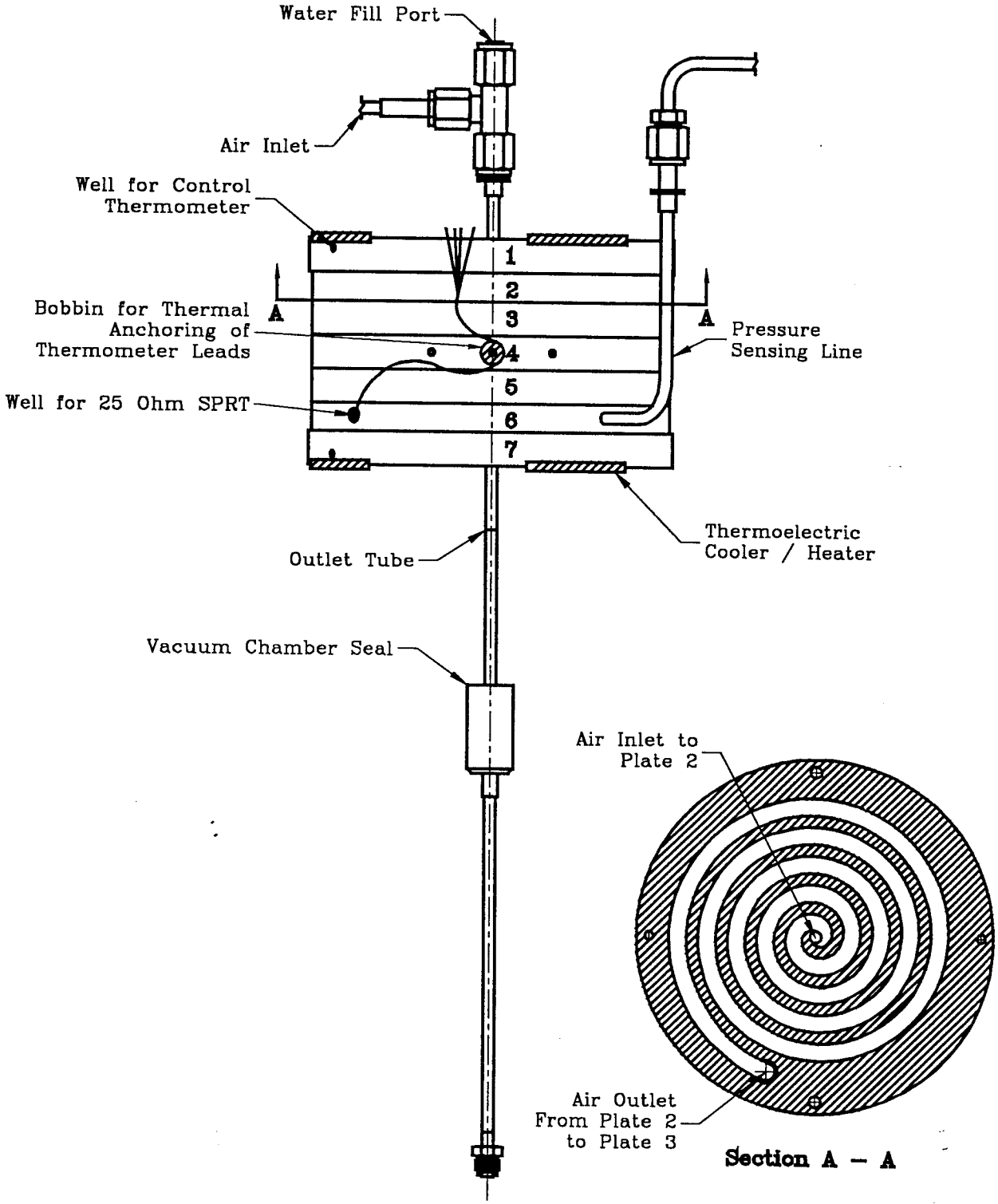


Fig. 2 Scaled diagram of the Low Frost Point Generator saturator system.

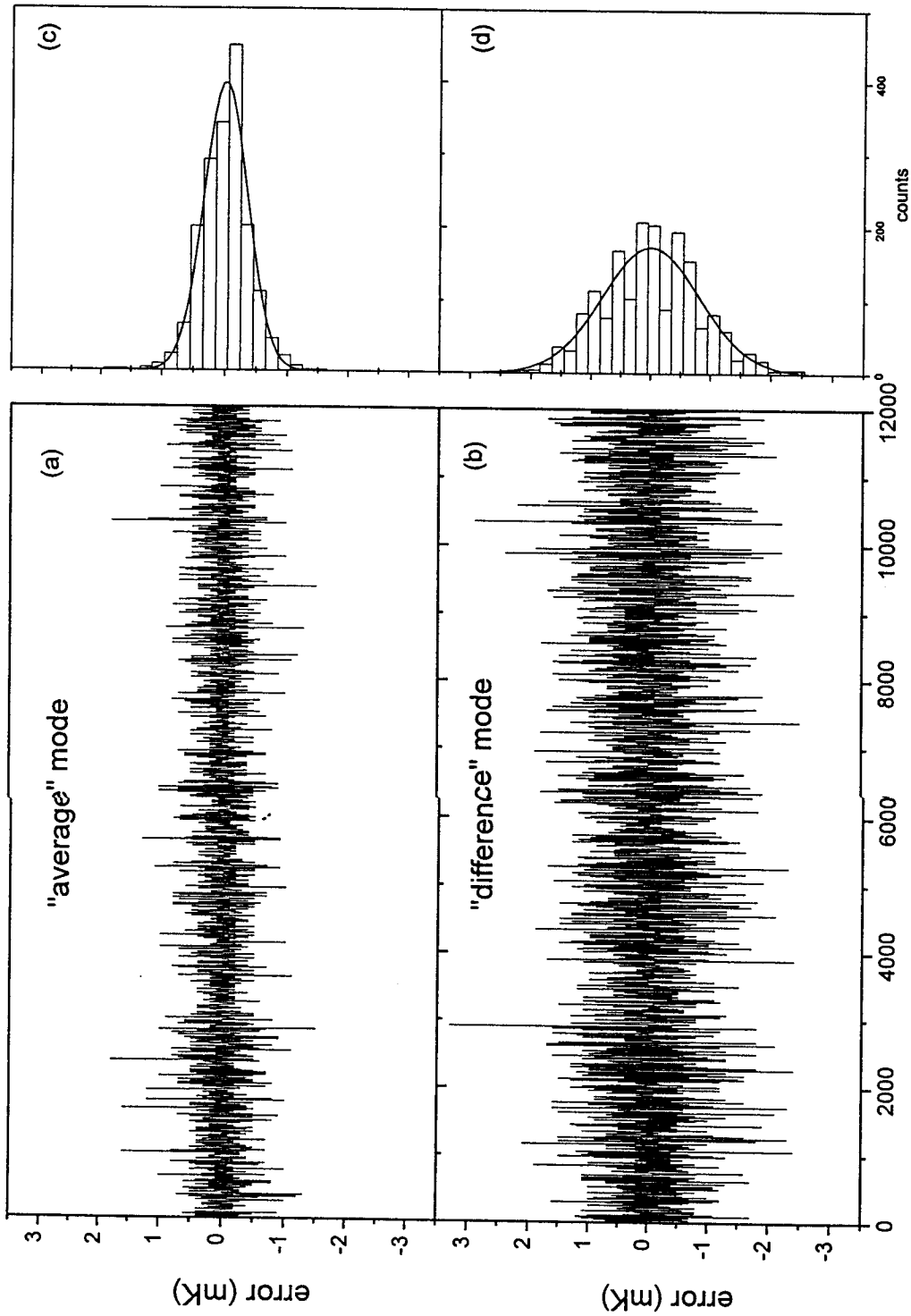


Fig. 3 Time response of the error signal associated with the saturator control thermometers in; (a) average mode and (b) difference mode. Figures (c) and (d) represent histograms of the data in (a) and (b), respectively. The smooth curves are Gaussian fits to these distributions.

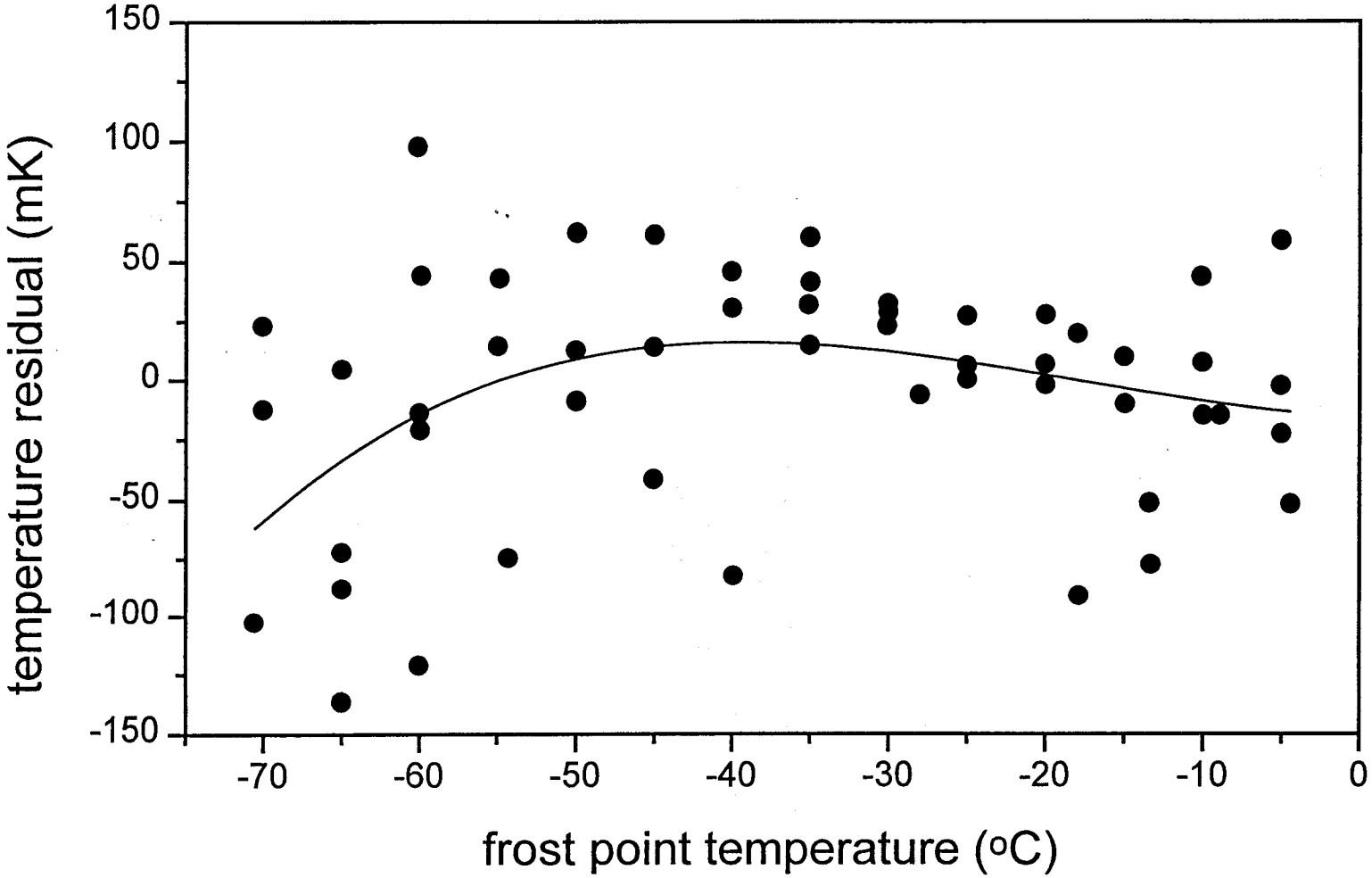


Fig. 4 The chilled mirror hygrometer calibration data (from the 2-P generator) reduced in terms of temperature residuals. The discrete symbols represent , $\delta t_{i,2-P}(t_i, R_i)$, and the horizontal axis is the predicted frost point temperature of the 2-P generator. The smooth curve is a third-order polynomial fit to the residuals corresponding to the interpolating function, $\delta t_{2-P}(q_0, q_1, q_2, q_3; t)$.

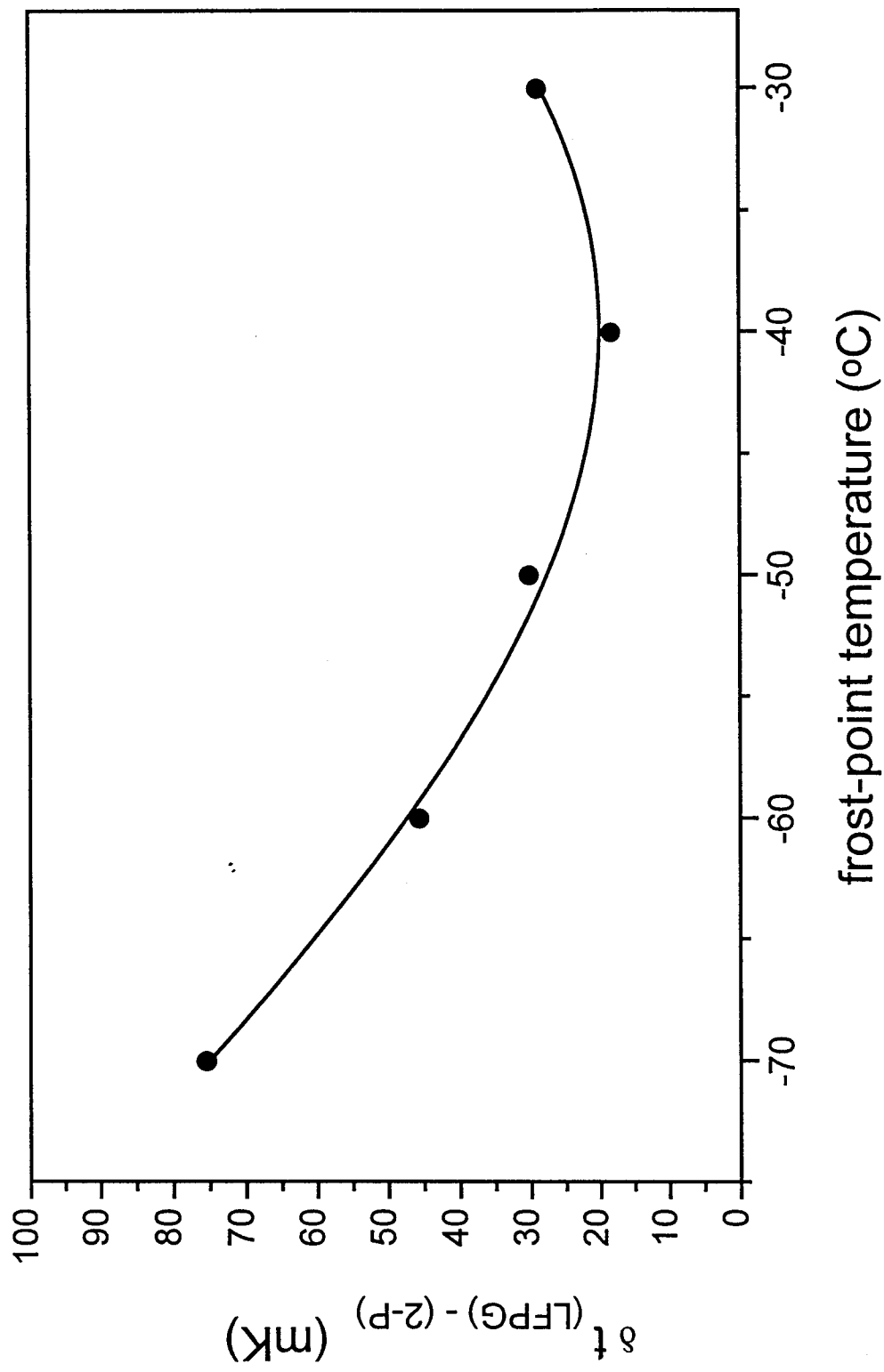


Fig. 5 Intercomparison of the measured LFPG and 2-P frost-point temperatures. The vertical axis is the difference, $\delta t_{(LFPG)-(2-P)}(R_f, t_f)$, defined in Eq. 6, and the horizontal axis is the frost-point temperature of the LFPG. The smooth line is a polynomial fit to the results.